ACS APPLIED MATERIALS & INTERFACES

Research Article

www.acsami.org

Fabrication of Transparent Nanohybrids with Heat Resistance Using High-Density Amorphous Formation and Uniform Dispersion of Nanodiamond

Muhammad Abdullah Al Mamun,[†] Youichi Soutome,[†] Yusuke Kasahara,[†] Qi Meng,[†] Shuichi Akasaka,[‡] and Atsuhiro Fujimori*[,†]

[†]Graduate School of Science and Engineering, Saitama University, 255 Shimo-okubo, Sakura-ku, Saitama 338-8570, Japan

[‡]Graduate School of Science and Engineering, Tokyo Institute of Technology, 2-12-1 Ookayama, Meguro-ku, Tokyo 152-8550, Japan

Supporting Information

ABSTRACT: A new technology for the production of transparent material using a "crystalline" polymer is proposed in the present study. Further, transparent and flexible crystalline polymer nanohybrid film containing well-dispersed nanodiamond filler was fabricated. Partially fluorinated crystalline polymer with switchboard-type lamellae results in high transparency as a consequence of the formation of a high-density amorphous structure based on high-temperature drawing just below the melting point at 110 °C. Although the formation of nanohybrid materials composed of fluorinated-polymer/organo-modified nanocarbon is generally difficult, we confirmed the formation, via melt-compounding, using atomic force microscopy and wide-angle X-ray diffraction. Even though the polymer matrix/nanodiamond hybrid has remarkable aggregation properties, a well-dispersed state was achieved because of improvement in wettability obtained through surface modification of filler. The resulting nanohybrid demonstrates transparency, increased thermal degradation temperature, and enhanced mechanical properties, which seem to be derived from the nucleation effect caused by the adsorption of the terminal polymer chain onto the organic modifier.

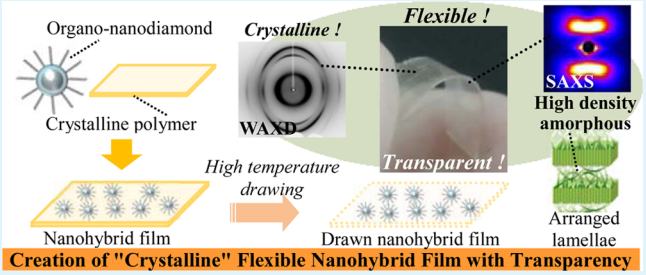

KEYWORDS: *"crystalline" partially fluorinated polymer, organo-surface modification, polymer/nanodiamond hybrid, transparent flexible film, high density amorphous*

INTRODUCTION

Can nanocarbons be dispersed into a polymer matrix? This question has not been answered yet. The trigger for this question has been the discovery of carbon nanotubes (CNTs).[1] For polymer nanocomposite materials made in 1987,[2] the use of CNTs as nanofillers[3] was a distant dream, and it is not surprising that many researchers have been unable to employ these materials successfully.[4,5] Nanodiamonds (NDs)[6,7] have many attractive features that can improve the physical properties of materials when they are included in nanocomposites. However, they have a remarkable ability to aggregate together, and this is the main hindrance to their use in nanocomposite materials. Therefore, in this study, we tried to develop a well-dispersed ND nanocomposite.

Transparent plastic films can be produced from crystalline plastics, after devitrification, by drawing an amorphous polymer film;[8] the drawing of polymers to achieve transparent films is a known process.[9,10] Generally, transparency in films is due to a highly amorphous polymer state. In crystalline polymers, the crystalline and amorphous regions are intermingled,[11−13] and light passing through the film is refracted at the crystalline/amorphous interfaces leading to an opaque plastic.[14,15] However, when the crystalline spherulites are smaller than the wavelength of light, it is not possible to obtain greater transparency. Consequently, several transparent plastics are not resistant above the glass transition temperature. For example, practical plastic optical fibers (POFs) have a resistance temperature of only 95 °C, and newer prototypes only up to 125 °C.[16] One of the primary aims of this paper is to develop a new heat-resistant (at 300 °C) transparent optical material. The key to this is the formation of switchboard lamellae.[17] Many perfluorinated and partially fluorinated polymers are crystalline and have rigid molecular chains; therefore, they may prove useful in forming switchboard lamellae. In this study, we have investigated the mechanism and origin of the transparency of these polymers.

Organic/inorganic hybrids[18] have captured the attention of scientists and engineers due to their high dimensional stability and gas-barrier performance[19] in addition to their superior mechanical properties[20] over conventional composite materials.[21] The use of NDs[6,7] in a wide range of products such as heat spreaders,[22,23] photonic crystals,[24] medical equipment, electronics,[25] sensors,[26] and biosensors due to properties such

Received: May 12, 2015
Accepted: July 17, 2015
Published: July 17, 2015

DOI: 10.1021/acsami.5b04083
ACS Appl. Mater. Interfaces 2015, 7, 17792−17801

as high thermal conductivity,[27] high refractive index,[28] antibacterial activity,[29] increased conductivity,[30,31] and nonphotobleaching fluorescence[32] has spurred research interest in these materials.

Fluorinated polymers are both water and oil repellent.[33] Thus, obtaining a uniform distribution of the nanofillers in the matrix is difficult.[34] Both hydrogenated materials and inorganic particles are phase-separated from the fluorinated polymers with no miscibility.[35] Additionally, perfluorinated and partially fluorinated crystalline polymers, such as PTFE (polytetrafluoroethylene),[36] PFA (poly(tetrafluoroethylene-*co*-[perfluoroalkylvinylether])),[37] FEP (perfluoro(ethylene-*co*-[propylene])),[38] and ETFE (poly(ethylene-*co*-[tetrafluoroethylene])),[39] have high melting points and are insoluble or sparingly soluble[40] in organic solvents. Nanohybrid formation by solution casting is almost impossible, and the melt-compounding method is also difficult to employ because the organo-modification to the surface of the filler, which improves the wettability toward organic polymers, thermally decomposes below the melting point of the polymer matrix.[41]

In this study, we attempt to resolve these problems using organo-modified NDs. The NDs were surface modified with a long-chain fatty acid.[42,43] As a result, we have obtained a new, heat-resistant, transparent, and flexible fluorinated polymer film. Heat-resistant films, with transparency and flexibility, produced by the formation of a high-density amorphous polymer containing a uniform dispersion of nanofillers, are expected to have wide applicability in industry. Fluoropolymers have several attractive inherent properties; these include chemical resistance,[44] weather resistance,[45] low surface energy (water repellency),[46] insulation,[47] chemical stability,[48] and flame retardancy.[49] The range of applications for these materials is wide and can be expanded by increasing their transparency, heat resistance, and flexibility. Possible applications include display boards,[50] solar-cell back-sheets,[51] and building window materials. Additionally, they could be used in next generation wearable technologies such as 3D-glasses if a highly transparent nanohybrid with a high refractive index can be produced.

EXPERIMENTAL SECTION

Materials. The partially fluorinated polymer used as the matrix in this study was P(VDF-TeFE) (see Supporting Information, Figure S1a). P(VDF-TeFE) has high melting point of 130 °C, a relatively low value of all the fluorinated polymers. Photographs in the Supporting Information show the differences between a perfluorinated polymer, PFA, a partially fluorinated polymer, ETFE, and P(VDF-TeFE) by drawing at high temperature just below the melting point five, three, and five times, respectively. From this result, fluorinated polymers with a rigid molecular chain are expected to form switchboard-type lamellae[9,10,17] (inset of Figure S1b); the materials became denser, and this indicates that the polymer chains are highly mobile. The nanocarbon nanoparticles used in this study correspond to ND (Figure S2). ND is obtained by pulverizing based on the bead milling process after detonation method. ND is covered by adsorbed nanolayers[22] of water to maintain the particle diameter within a magnitude of nanometer size. Although NDs are purchased products (New Metals and Chemicals Corporation), this is manufactured by Nano Carbon Institute of Shinshu University. Details of the production have previously reported by E. Osawa.[52] NDs are spherical nanoparticles of 4−5 nm size. The surfaces of the NDs were modified with stearic acid, hereafter described as organo-modification.[53,54] Bond formation by long-chain fatty acids was supported by the lack of COO^- band by infrared (IR) measurement. The thermal decomposition temperature of organo-ND was about 155 °C. Because of this thermal stability, a melt-compounding process was used to construct the P(VDF-TeFE)/organo-modified-ND material. Previous studies[55] have shown that in similarly organo-modified nanocomposites of PFA/organo-modified-smectite, or organo-modified mica, the nanoclay is dispersed uniformly. By using these novel fatty acid surface modification techniques, there is no example of composite formation after the converting from the ND to the organo-modified ND. Surface modification techniques of ND itself are a new technology. This technique is expected to the effect of suppressing the high cohesion of traditional nanocarbon-based filler. P(VDF-TeFE)/organo-modified-ND were extruded at 145 °C using a twin-screw extruder (Labo kneader mill, Toshin Co., Ltd.) (Figure S3). The content of organo-modified ND in the nanohybrid material was 0.2 and 1.0 wt %. We also prepared nanohybrids containing 2.0 and 3.0 wt % ND for comparison. The P(VDF-TeFE) and its nanohybrid were molded into 500 μm films between two polyimide sheets (Kapton1 HN, Toray-DuPont Co., Ltd.) using a hot press at 145 °C and at 20 MPa for 5 min and then quenched to room temperature. The melt-quenched film specimen (width, 20 mm; length, 30 mm) cut from these films was drawn using a hand-drawing apparatus in an air oven at 110 °C. The surface of the film specimen was marked at intervals of 1 mm to measure the draw ratio. The drawing speed was fixed at 10 mm/min, and the film was annealed at 110 °C for 5 min before drawing.

Procedures. *Estimation of the Dispersion State of Organo-ND in the Polymer Matrix.* To estimate the dispersion state (Figure 1) of organo-ND in the polymer matrix, we used atomic force microscopy (AFM) (SPA300 with an SPI-3800 probe station. Seiko Instruments Inc.) and transmission electron microscopy (TEM) (Hitachi H-7650 Zero A, accelerating voltage 120 kV, sample thickness 60 nm).

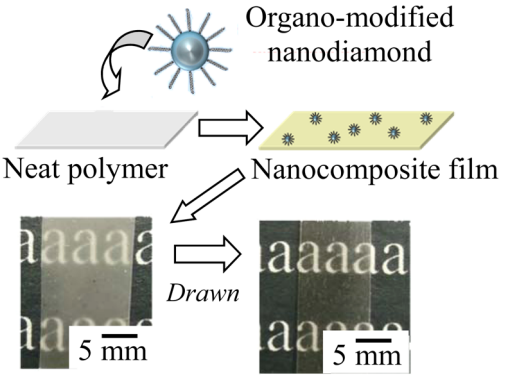

Figure 1. Schematic illustration of the formation of transparent crystalline polymer/organo-ND hybrid film prepared by the high-temperature drawing.

Evaluation of the Crystal Structure and Packing. To evaluate the crystal structure, packing, and crystallite size of the neat P(VDF-TeFE)s and the nanohybrids, we used wide-angle X-ray diffraction (WAXD). The diffractometer (R-axis Rapid diffractometer. Rigaku Co. Ltd.) was operated at 45 kV and 200 mA to generate Cu Kα radiation (λ = 0.1542 nm).

Estimation of the Long Periods of Lamellae and Difference between Electron Density of Crystal Amorphous Regions. We used small-angle X-ray scattering (SAXS) to estimate the long periods of lamellae and the difference between the electron density of the crystalline and amorphous regions of the drawn and undrawn neat P(VDF-TeFE) and the nanohybrids. The diffractometer (Nanoviewer. Rigaku Co. Ltd.) was operated at 40 kV and 30 mA to generate Cu Kα radiation (λ = 0.1542 nm).

Examination of Thermal Behavior Relative to Phase Transition. The thermal properties of neat P(VDF-TeFE) and the nanohybrids were examined by differential scanning calorimetry (DSC) using a DSC-6200 with an EXSTAR6000 station (Seiko Instruments Inc.) in the range of 50−155 °C, at a heating rate of 10 °C min^{-1}. In each DSC run, the sample (approximately 3.0 mg) was heated. To estimate the degree of crystallinity from the heat of fusion data, we employed the

DOI: 10.1021/acsami.5b04083
ACS Appl. Mater. Interfaces 2015, 7, 17792−17801

value of 104.6 J/g for the melting enthalpy of 100% crystalline polyvinylidene fluoride (PVDF).

Spherulite Observation. To observe the spherulite morphology of neat P(VDF-TeFE) and the nanohybrids, we used a polarized optical microscope (POM) (BH-2 polarizing microscope, Olympus Co. Ltd.) equipped with a video camera system. A hot-stage (Linkam THM-600) was also utilized to measure the spherulite growth rates.

Measurement of Mechanical Properties. To examine the mechanical properties of neat P(VDF-TeFE) and the nanohybrids by strain−stress measurements, a TMA/SS-6000 with EXSTAR6000 station (Seiko Instruments Inc.) was utilized. Dynamic mechanical analysis (DMA) (Rheology Ltd. DVE-V4FT Leo Spectra) was used with measurement mode: dynamic viscoelasticity and temperature dependence. Frequency, 1 Hz; amplitude variation, 6 μm; heating rate, 5 °C min^{-1}; range, 30−320 °C.

Estimation of the Changes in the Thermal Degradation Temperature. The thermal decomposition behavior of the neat P(VDF-TeFE) and its nanohybrids was examined by thermogravimetric analysis (TG/DTA-6100 with EXSTAR6000 station. Seiko Instruments Inc.) under N_2 gas in the range 50−500 °C at a heating of 10 °C min^{-1}.

RESULTS AND DISCUSSION

Formation of Partially Fluorinated "Crystalline" Copolymer/Organo-Modified ND Hybrid at Uniform Dispersion.[56,57] Figure 2, panel a shows an AFM image of

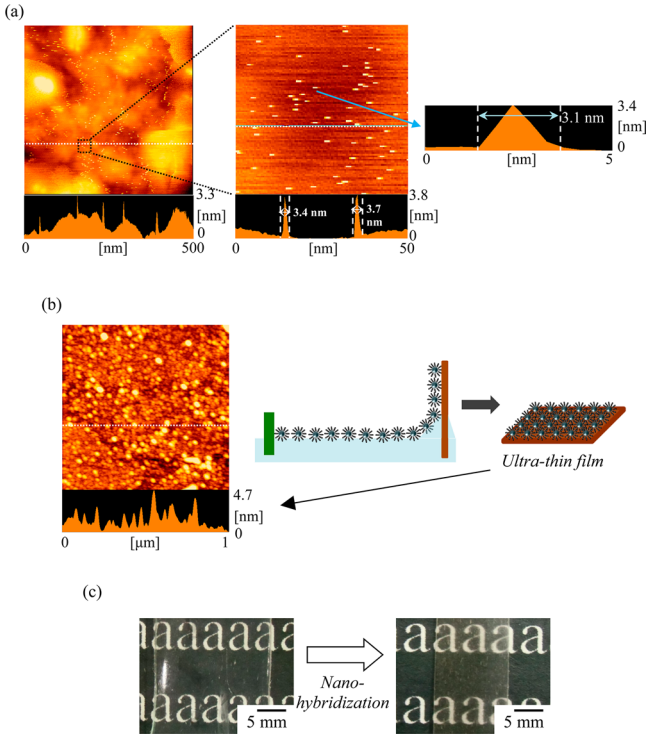

Figure 2. (a) AFM image of P(VDF-TeFE) nanohybrid containing 0.2 wt % organo-ND. (b) AFM image of Langmuir−Blodgett monolayer of organo-ND. (c) Photograph of drawn and undrawn of P(VDF-TeFE) nanohybrid film containing 0.2 wt % organo-ND.

the surface of the press-molded film of P(VDF-TeFE)/organo-modified ND hybrids that were made by melt-compounding. The sample was cooled to 110 °C after being melted at 150 °C, and the free surface was observed. Figure 2, panel a indicates that there are relatively hard nanoparticles in the polymer matrix. Both the height and the width of the nanoparticles are approximately 4 nm. This is approximately the same as the height information derived from the Langmuir−Blodgett film of organo-modified NDs (Figure 2b).[58] Further, the transparency of the "crystalline" partially fluorinated polymer nanohybrid has been retained (Figure 2c). This indicated that the organo-modified NDs are uniformly dispersed throughout the fluorinated polymer matrix formed by melt-compounding with P(VDF-TeFE).

We cannot investigate how the NDs are dispersed in the inner matrix using AFM. Therefore, a comparison of WAXD profiles of organo-modified ND, neat P(VDF-TeFE), and their nanohybrids was performed (Figure 3). The WAXD profiles of

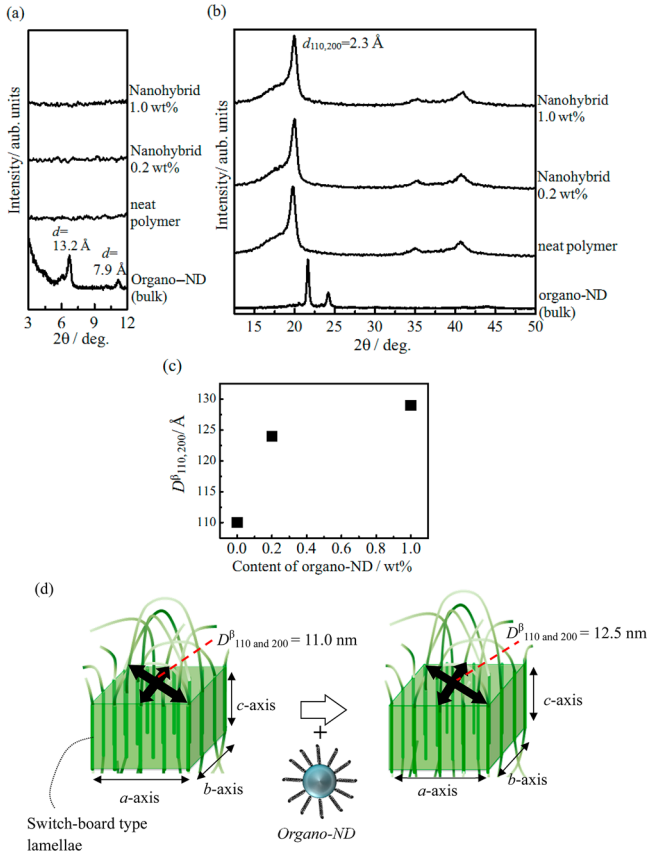

Figure 3. WAXD profiles of organo-ND in bulk, P(VDF-TeFE) nanohybrids containing 0.2 and 1.0 wt % organo-ND [(a): 3−12°, and (b): 12−50°]. (c) Plot of content of organo-ND in polymer metrix versus crystallite size by Scherrer equation. (d) Schematic illustration of changes in crystallite size along the *ab*-plane by organo-ND addition.

the organo-modified NDs show clearly the low angle (00*l*) reflection. This indicates that a layered structure is formed in the bulk state (see Figure 3a). Here, because we do not observe reflections from this layer structure at low angle in the nanohybrids with different filler contents, we believe that the modified NDs are uniformly distributed throughout the polymer matrix. Figure 3, panel b shows the high angle diffraction data; the position of the reflections, and therefore *d*, is independent of the filler content. Therefore, addition of a filler does not cause a change in the crystal structure. However, the average crystallite size, calculated from the Scherrer equation, gradually increases and is dependent on the ND content (Figure 3c). Here, the reflection of the highest intensity at around $2\theta = 20°$ was used. As we will further describe later, this is a combined peak from diffraction from the (110) and (200) planes of the β-form crystal of P(VDF-TeFE). The average diameter of crystallites perpendicular to the (110) and (200) planes has been approximately calculated (Figure 3d).

DOI: 10.1021/acsami.5b04083
ACS Appl. Mater. Interfaces 2015, 7, 17792−17801

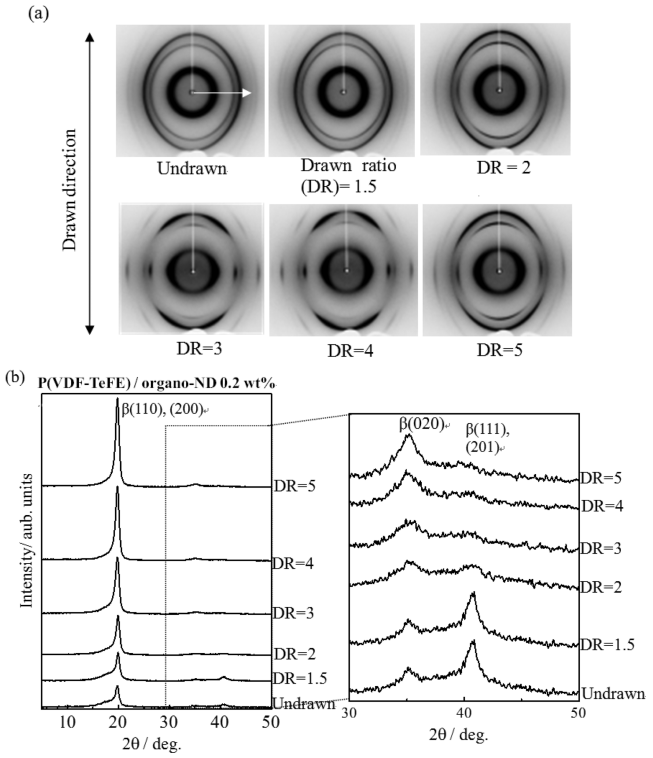

Figure 4. (a) WAXD patterns of drawn and undrawn P(VDF-TeFE) nanohybrids containing 0.2 wt % organo-ND. (b) WAXD profiles of drawn and undrawn P(VDF-TeFE) nanohybrids containing 0.2 wt % organo-ND.

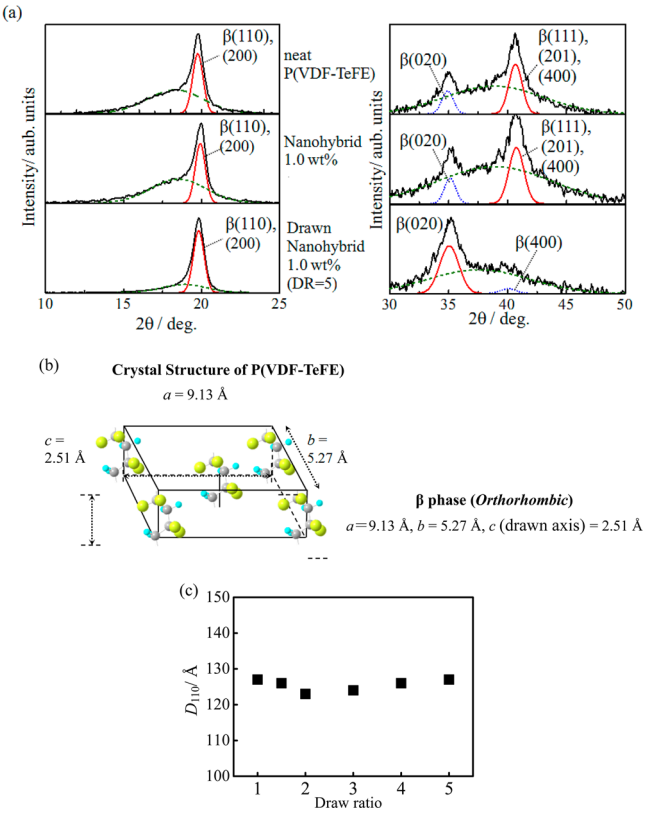

Figure 5. (a) Deconvolution and curve fitting of WAXD profiles of neat P(VDF-TeFE) and the drawn nanohybrids containing 1.0 wt % organo-ND. (b) Crystal structure of P(VDF-TeFE) used in this study. (c) Plots of $D^{\beta}_{(110),(200)}$ crystalline size versus the draw ratio of a P(VDF-TeFE) nanohybrid containing 0.2 wt % organo-ND.

In addition, although it was found that an ND was almost single particle dispersion in the vicinity of the surface by AFM observation, it was observed that there were also aggregates on the order of 100 nm in internal matrix by TEM observation (Figure S4). From the experimental fact that WAXD reflection is not confirmed, it will be considered as aggregates with low regularity. Therefore, because of the weak interaction between particles, dispersibility may be improved by devising kneading technique. In addition, it does not inhibit transparency since aggregates size corresponds below wavelength of visible light.

Fine Structural Analysis of "Crystalline" Transparent Nanohybrid with ND. Figure 4 shows WAXD patterns and profiles of drawn and undrawn P(VDF-TeFE) nanohybrids containing organo-ND. We have used WAXD to estimate the fine structure at the subnanometer scale. The WAXD patterns show strong arc-shaped spots along the equator line of the draw axis (Figure 4a) and integrated profiles along the equatorial direction are shown in Figure 4, panel b. The maximum intensity of the reflections occurs at around $2\theta = 20°$. In addition, a small peak at around $2\theta = 35°$ systematically increases with increasing draw ratio. Conversely, the diffraction intensity of the peak at around $2\theta = 40°$ systematically decreases with the increasing draw ratio, and since these peaks exist on the equator line, the diffraction intensity related to the *c*-axis, conincident with the draw axis, decreases.

Figure 5, panel a shows the analysis of the diffraction patterns with respect to the crystal structure after nanohybrid formation. On the basis of Figure 4, panel b, we determined that a transition in the crystal system after formation of the nanohybrid did not occur. Only the β-form of the PVDF copolymer crystals shows ferroelectric properties.[59] Thus, it would be advantageous to maintain the β-form to add ferroelectric properties to the properties of the composites. Figure 5, panel a shows the deconvolution of the amorphous curve (halo) from the crystalline reflections. The reflection at $2\theta = 20°$ is considered to be a combination of the (110) and (220) reflections of the β-form.[60] The α-form has characteristic peaks at $2\theta = 17°$ and 19°.[61] Similarly, the deconvoluted reflection at $2\theta = 35°$ is considered to arise from the β-form crystal (020) plane. In addition, although the reflection at around $2\theta = 40°$ could be a combined peak from the β-form crystal (111) and (201) reflections, we considered that these are the β-form (400) reflection. This suggests that the β-form is maintained in P(VDF-TeFE) matrix and therefore so is ferroelectricity. In addition, we found that the crystallite size is constant at different draw ratios indicating that $D^{\beta}_{(110),(200)}$ is not dependent on the draw ratio (Figure 5c).

Figure 6 shows SAXS patterns and profiles of drawn and undrawn P(VDF-TeFE) nanohybrids containing 0.2 wt % organo-ND. The undrawn hybrid exhibited a circular scattering pattern (Figure 6a), and the profile obtained by integrating along the equator line direction indicates a long period of 20.7 nm (Figure 6b). In accordance with the drawing process, scattering images have gradually changed to a four-point scattering image from symmetric scattering via a two-point scattering image (Figure 6a). The analysis of these data indicates that the lamellae transition from an initial isotropic state to an arrangement parallel to the draw direction, finally forming a herringbone array[9,10] (Figure 6c).

Also, in the SAXS diffraction patterns of the nanohybrids that have been subject to drawing, the SAXS intensity significantly

DOI: 10.1021/acsami.5b04083
ACS Appl. Mater. Interfaces 2015, 7, 17792−17801

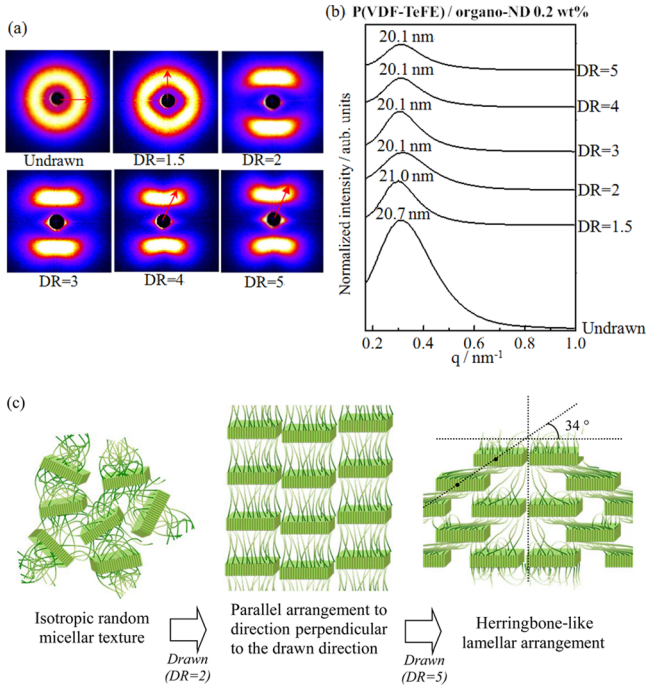

Figure 6. (a) SAXS patterns of drawn and undrawn P(VDF-TeFE) nanohybrids containing 0.2 wt % organo-ND. (b) SAXS profiles of drawn and undrawn P(VDF-TeFE) nanohybrids containing 0.2 wt % organo-ND. (c) Schematic illustration of the model of lamellar arrangement in the P(VDF-TeFE) nanohybrid containing 0.2 wt % organo-ND.

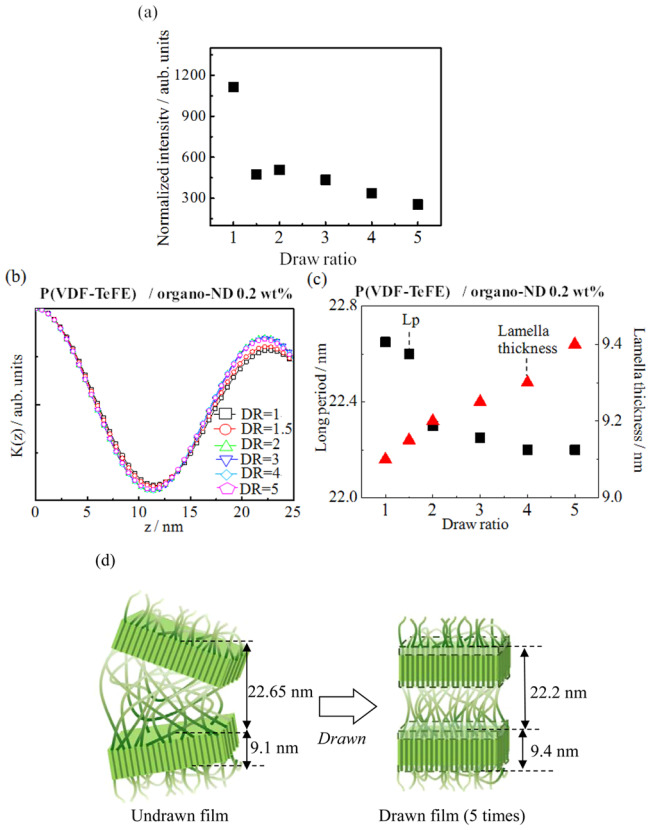

Figure 7. (a) Plots of the normalized SAXS intensity versus draw ratio of P(VDF-TeFE) nanohybrids containing 0.2 wt % organo-ND. (b) Correlation function in one-dimensional density $K(z)$ of drawn P(VDF-TeFE) nanohybrids with 0.2 wt % organo-ND. (c) Plots of L_p (distance between lamellae interfaces) and distance between the center of gravities of lamellae crystal parts versus drawn ratio of P(VDF-TeFE) nanohybrid containing 0.2 wt % organo-ND calculated using the correlation function of the one-dimensional density. (d) Schematic illustration of changes in lamellae structure by the high-temperature drawing.

decreases between the undrawn and the 1.5 times drawn samples (Figure 7a). The SAXS intensity along the vertical axis reflects the difference in electron density between crystal and amorphous regions.[62] That is to say, the amorphous density is expected to increase on high-temperature drawing. Figure 7, panel b shows the normalized one-dimensional electron density correlation functions, calculated according to Stroble's method,[63−65] from the SAXS profiles of the drawn nanohybrids that contain 0.2 wt % ND. Figure 7, panel c also summarizes the structural parameters from this analysis. From these data, it is possible to make a quantitative evaluation. These results indicate that long period (L_p), the distance between the lamellae in the nanohybrids, gradually decreases from 22.7 to 22.2 nm after high-temperature drawing, while the thickness of the crystalline part along the *c*-axis increased from 9.1 to 9.4 nm (Figure 7d). The normalized intensity along the vertical SAXS axis decreased at larger draw ratios; this indicates an increase in the amorphous density. However, the L_p value is simultaneously reduced, while the crystal thickness is increased. Therefore, since the denser amorphous component gradually becomes crystalline and the distance between lamellae decreases, in the amorphous density increases. Because high amorphous density is associated with greater transparency, this contributes to a more transparent material.

However, increasing the filler content has an opposing effect to drawing. Depending on the quantity of ND that is added, the SAXS intensities increase almost linearly (see Figure 8a). Although quantitative analysis of the normalized one-dimensional electron density correlation function shows substantially similar results, that is, lamellar thickening, the cause of this is unclear.

Figure 9 shows the results of DSC measurements of neat P(VDF-TeFE) and the nanohybrids containing organo-ND. The thermodynamic parameters are summarized in Table 1. The thermograms indicate that the improvement in crystallization temperature is dependent on the quantity of ND added. As in the case of the nanohybrid with 0.2 wt % filler content, the crystallization temperature increases by only 0.2 °C, whereas that with 1.0 wt % nanohybrid rises by 0.5 °C from the crystallization temperature of neat P(VDF-TeFE).

Figure 10 shows POM images of spherulites of neat P(VDF-TeFE) and the nanohybrid with 1.0 wt % ND content. These images indicate that the improvement in crystallization temperature and thickening of lamellae (as indicated by the SAXS data) are caused by a "nucleation" effect, initiated by the organo-modified ND in the P(VDF-TeFE) copolymer. To clarify, the spherulites are finer, and the density of the nuclei is greater. P(VDF-TeFE) does not terminate in a fluorinated functional group, and so active groups still may be present. Therefore, the terminal groups of the polymer chain can adsorb to part of the stearic acid molecules on the surface of the NDs, initiating nucleation. The *b*-axis length of crystalline P(VDF-TeFE) (5.27 Å) and the *a*-axis length of crystalline stearic acid (5.59 Å) are similar; because of this, it is possible that heterogeneous nucleation occurs by epitaxial growth.

Improvement Behavior of Physical Properties of "Crystalline" Transparent Nanohybrid with ND. Figure 11 shows the improvement in the thermal degradation temperature of the samples treated in this study by measurement of the TG

DOI: 10.1021/acsami.5b04083
ACS Appl. Mater. Interfaces 2015, 7, 17792−17801

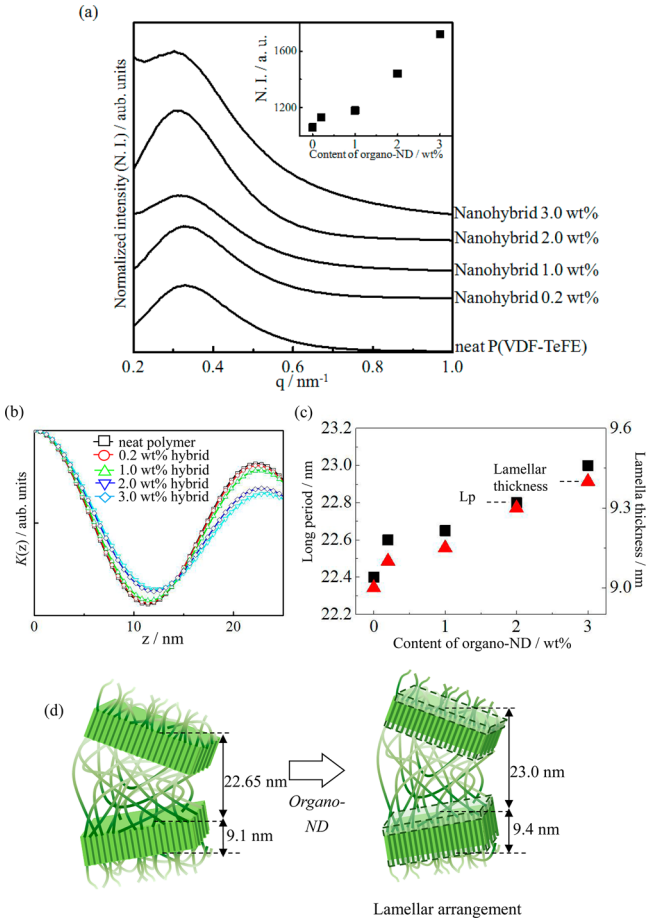

Figure 8. (a) SAXS profiles of P(VDF-TeFE) nanohybrids containing several organo-ND contents. (inset) Plot of normalized intensity versus nanofiller content. (b) Correlation function in one-dimensional density $K(z)$ of P(VDF-TeFE) nanohybrids with several ND contents. (c) Plots of L_p (distance between lamellae interfaces) and the distance between centers of gravity of the lamellae crystal parts versus nanofiller content. (d) Schematic illustration of changes in lamellae structure by the nanohybridization.

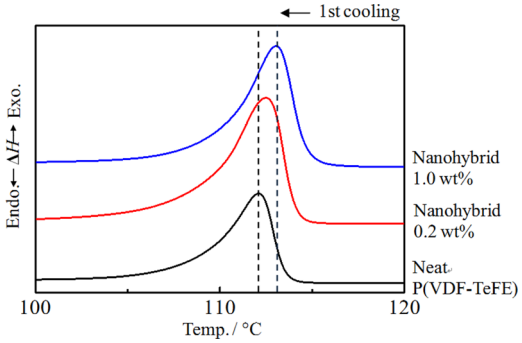

Figure 9. DSC thermograms of neat P(VDF-TeFE) and P(VDF-TeFE) nanohybrids containing 0.2 and 1.0 wt % organo-ND.

curve. The thermal degradation parameters and their activation energy, calculated from an Ozawa plot,[66] are shown in Table 2. In comparison with neat P(VDF-TeFE), both 5% and 10% weight loss temperature of undrawn nanohybrid is improved to 14 °C. For the nanohybrid that was drawn five times, both the 5% and 10% weight loss temperatures are increased to 19 and 20 °C, respectively. In addition, the activation energy for thermal

Table 1. Thermodynamic Parameters Derived from DSC Data of Neat P(VDF-TeFE) and Their Nanohybrids with 0.2 and 1.0 wt % Organo-ND

	crystalline temperature [°C]	degree of crystallinity [%]
neat P(VDF-TeFE)	112.7	17.5
P(VDF-TeFE)/organo-ND 0.2 wt %	112.9	20.2
P(VDF-TeFE)/organo-ND 1.0 wt %	113.2	21.6

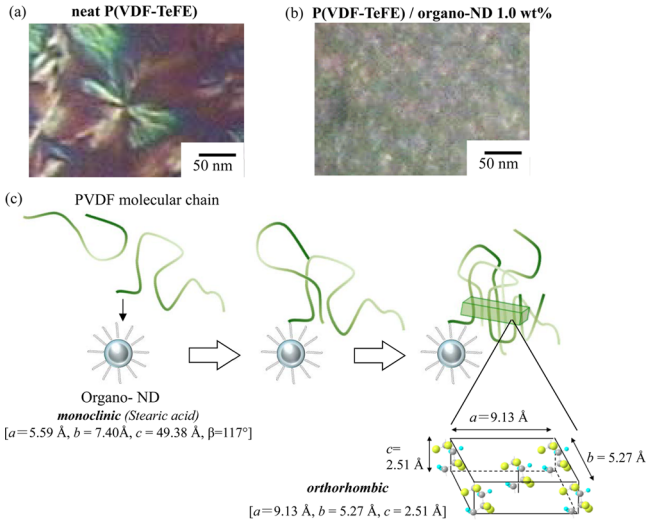

Figure 10. Polarized optical micrographs of (a) neat P(VDF-TeFE) and (b) P(VDF-TeFE) nanohybrid containing 1.0 wt % organo-ND. (c) Schematic illustration of the nucleation effect between P(VDF-TeFE) polymer chain and organo-ND.

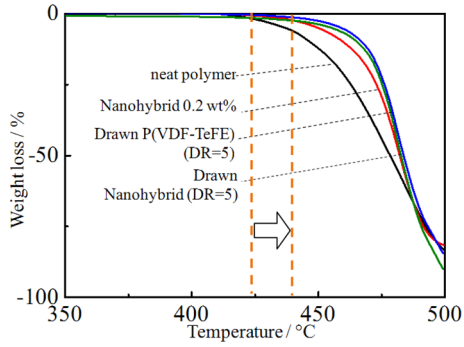

Figure 11. TG curves of neat P(VDF-TeFE), undrawn P(VDF-TeFE)/organo-ND nanohybrid (0.2 wt %), drawn P(VDF-TeFE) (five-times drawing), and drawn nanohybrid (0.2 wt % content and five-times drawing).

degradation is increased from 67.2 to 75.0 kJ/mol by nanohybridization and drawing. Because nucleation increases the nuclear density[67,68] in the drawn nanohybrids, the increase in thermal degradation temperature is an expected result.

The increase in the thermal decomposition temperatures is related to the high-density amorphous regions that remain even after the melting of the crystalline regions. The high-density amorphous regions remain even above the melting point of 130 °C. The fact that the amorphous polymers do not have a sharply defined melting point further contributes to the improvement in the decomposition temperature. Furthermore, from a comparison of Figure 3, panel c, the size of crystallites in the *ab*-plane is increased on the addition of organo-ND.

DOI: 10.1021/acsami.5b04083
ACS Appl. Mater. Interfaces 2015, 7, 17792−17801

Table 2. Decomposition Temperatures (50% Weight Loss) and Activation Energies Calculated from TG Curves of Drawn and Undrawn Neat P(VDF-TeFE) and Their Nanohybrids with 0.2 wt % Organo-ND

	decomposition temperature (50%) [°C]	activation energy [kJ/mol]
neat P(VDF-TeFE)	478	67.2
P(VDF-TeFE) nanohybrid 0.2 wt %	483	73.2
drawn P(VDF-TeFE) (*DR* = 5)	484	75.0
drawn nanohybrid 0.2 wt % (*DR* = 5)	484	75.2

The increase in the crystallite size along the in-plane direction is not caused by drawing but occurs on addition of organo-ND. In the case of the increase in crystallite size, the expansion of the high-density amorphous component also occurs in the *ab*-plane. As a result, oxygen molecules are less likely to penetrate inside the material in at high temperature and thus improves the thermal decomposition temperature.

Preliminary TG measurements in an oxygen atmosphere suggest that drawing does not increase the thermal decomposition temperature, but nanohybridization does. The increase in crystallite size in the *ab*-plane leads to greater high-density amorphous content, and this acts as a barrier to thermal decomposition by oxygen, which raises the decomposition temperature.

Figure 12 shows the evaluation of macroscopic mechanical properties of the nanohybrids used in this study by DMA and

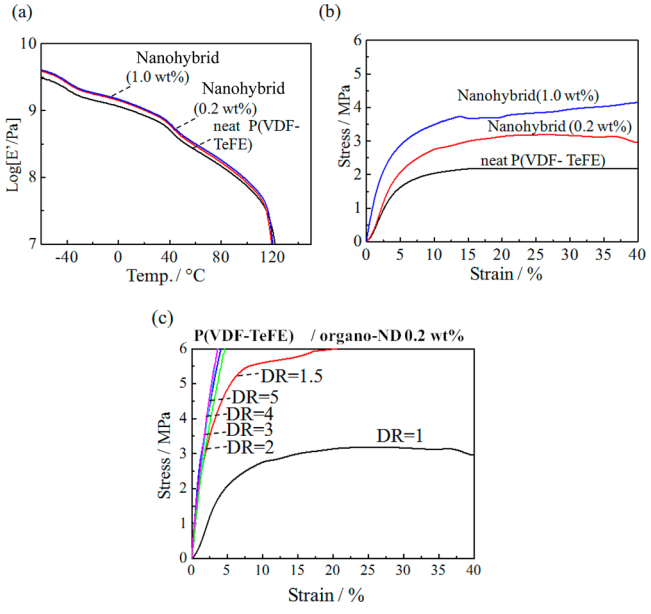

Figure 12. (a) Comparison in the content of organo-ND of dependence on the storage modulus of P(VDF-TeFE) nanohybrids by DFM measurement. (b) Comparison of strain−stress curves in the content of organo-ND of dependence on the storage modulus of P(VDF-TeFE) nanohybrids. (c) Strain−stress curves of drawn and undrawn P(VDF-TeFE) nanohybrids containing 0.2 wt % organo-ND.

the measurement of strain−stress curve. Figure 12, panel a shows that the increase in storage modulus on nanohybridization is dependent on the amount of nanofillers added. The DMA results indicate that dimensional stability increased after nanohybridization. Figure 12, panel b shows that nanohybridization increased the Young's modulus. The values of Young's

Table 3. Young's Modulus Calculated by Strain−Stress Curves of Neat P(VDF-TeFE) and Drawn and Undrawn P(VDF-TeFE) Containing 0.2 and 1.0 wt % Organo-ND

	draw ratio	Young's modulus [MPa]
neat P(VDF-TeFE)	1	0.26
P(VDF-TeFE)/organo-ND 1.0 wt %	1	0.72
P(VDF-TeFE)/organo-ND 0.2 wt %	1	0.45
	1.5	2.2
	2	2.7
	3	2.8
	4	2.9
	5	3.2

modulus calculated from the initial slope are summarized in Table 3. Of the nanohybrids, both the Young's modulus and tensile strength vary between 1.5 and 2-times drawing (Figure 12c). In other words, we suggest that the dispersion of nanofillers, the formation of high-density amorphous regions, and improvement of the nuclear density by the nucleation effect have contributed to the enhancement of the mechanical properties and transparency in the 1.5 times drawn sample. As the polymers are drawn, the crystallites become oriented with respect to the drawing direction, and the tension is increased in the 1.5 times drawn sample, indicating an extreme enhancement of the mechanical properties.

Figure 13 summarizes the origin and mechanism of the formation of transparent, flexible plastics films, with heat

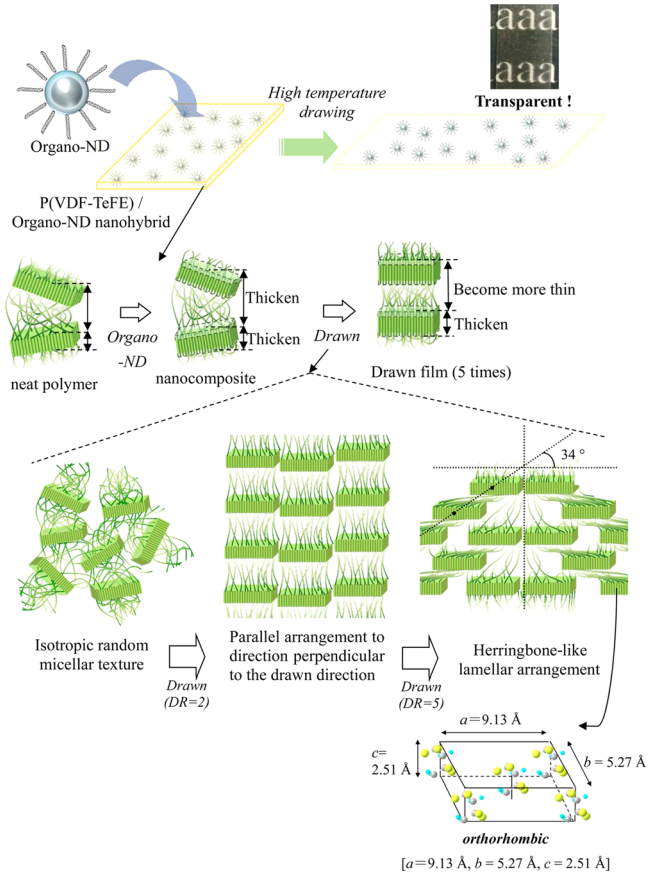

Figure 13. Schematic illustration of formation mechanism and fine structure of transparent and flexible fluorinated nanohybrid with heat-resistance obtained in this study.

DOI: 10.1021/acsami.5b04083
ACS Appl. Mater. Interfaces 2015, 7, 17792−17801

resistance. Partially fluorinated crystalline polymers became transparent and formed high-density amorphous regions on drawing at high-temperature. Nanohybrid formation allows the formation of a uniformly dispersed state. The nucleation density is also improved by virtue of an increased nucleation effect, and this leads to an increased thermal degradation temperature. Therefore, it is understood that hierarchical changes have been induced from the region of "the fine structure at nanometer-scale evaluated by the WAXD and SAXS" to "the macroscopic properties estimated by TG and mechanical properties".

CONCLUSIONS

We proposed that the use of switchboard lamellae in "crystalline" partially fluorinated polymers could lead to films with novel and improved properties. Surface-modified NDs were incorporated into P(VDF-TeFE) forming a nanohybrid material that, after high-temperature drawing, was transparent and heat resistant. The presence of switchboard lamellae in P(VDF-TeFE) leads to a high degree of transparency in the final film due to the formation of a high-density amorphous phase. Flexibility is a characteristic also determined by the presence of this phase and is retained after nanohybridization. If the matrix polymer is subject to nanohybridization and high-temperature drawing the β-form crystal, which has ferroelectric properties, it is also retained. The SAXS data indicate that high-temperature drawing contributed to an increase in the amorphous density and that nanohybridization causes thickening of the crystalline part of the lamellae. The increase in the nucleation density leads to an improvement in the mechanical properties and thermal degradation temperature. The nanostructure of drawn polymer films is hierarchical, and changes to the nanometer scale structure result in changes in the macroscopic properties. Thus, we have created a new material using this simple method, which can produce materials with improved heat-resistance, transparency, and flexibility.

ASSOCIATED CONTENT

Supporting Information

Characterization of transparent films of fluorinated crystalline polymers, characterization of organo-modified ND, procedure of melt-processing and film compression, and TEM images of nanocomposite materials. The Supporting Information is available free of charge on the ACS Publications website at DOI: 10.1021/acsami.5b04083.

AUTHOR INFORMATION

Corresponding Author

*E-mail: fujimori@fms.saitama-u.ac.jp. Phone: +81-48-858-3503. Fax: +81-48-858-3503.

Notes

The authors declare no competing financial interest.

ACKNOWLEDGMENTS

The authors greatly appreciate The Ministry of Education, Culture, Sports, Science, and Technology (MEXT) for Grant-in-Aid for Scientific Research (C, 25410219 (A.F.)). The authors also thank Takahiro Kikkawa and Nanami Honda, Saitama University for their assistance with data analysis. Finally, the authors offer their heartfelt condolences to Professor Kiyoshige Fukuda, Saitama University, a mentor, who died on July 7, 2015.

REFERENCES

(1) Iijima, S.; Ichihashi, T. Single-Shell Carbon Nanotubes of 1 nm Diameter. *Nature* **1993**, *363*, 603−605.
(2) Fukushima, Y.; Inagaki, S. Synthesis of an Intercalated Compound of Montmorillonite and 6-Polyamide. *J. Inclusion Phenom.* **1987**, *5*, 473−482.
(3) Du, F.; Scogna, R. C.; Zhou, W.; Brand, S.; Fischer, J. E.; Winey, K. I. Nanotube Networks in Polymer Nanocomposites: Rheology and Electrical Conductivity. *Macromolecules* **2004**, *37*, 9048−9055.
(4) Dong, S. R.; Tu, J. P.; Zhang, X. B. An Investigation of the Sliding Wear Behavior of Cu-Matrix Composite Reinforced by Carbon Nanotubes. *Mater. Sci. Eng., A* **2001**, *313*, 83−87.
(5) Kim, K. T.; Cha, S. I.; Hong, S. H. Hardness and Wear Resistance of a Carbon Nanotube Reinforced Cu Matrix Nanocomposites. *Mater. Sci. Eng., A* **2007**, *449-451*, 46−50.
(6) Branson, B. T.; Beauchamp, P. S.; Beam, J. C.; Lukehart, C. M.; Davidson, J. L. Nanodiamon Nanofluids for Enhanced Thermal Conductivity. *ACS Nano* **2013**, *7*, 3183−3189.
(7) Morimune, S.; Kotera, M.; Nishino, T.; Goto, K.; Hata, K. Poly(vinyl alcohol) Nanocomposites with Nanodiamond. *Macromolecules* **2011**, *44*, 4415−4421.
(8) Müllen, K.; Kobayashi, S. *Encyclopedia of Polymeric Nanomaterials*; Springer: New York, 2015.
(9) Fujimori, A.; Hayasaka, Y. Changes in Arrangement of Lamella and Fine Crystallite in Fluorinated "Crystalline" Transparent Fibers with Drawing. *Macromolecules* **2008**, *41*, 7606−7615.
(10) Fujimori, A.; Numakura, K.; Hayasaka, Y. Changes in Lamellar Arrangement of Crystalline and Flexible Fluorinated Transparent Tilms with Drawing. *Polym. Eng. Sci.* **2010**, *50*, 1295−1305.
(11) Keller, A. A Note on Single Crystals in Polymers: Evidence for a Folded Chain Configuration. *Philos. Mag.* **1957**, *2*, 1171−1175.
(12) Till, P. H. The Growth of Single Crystals of Linear Polyethylene. *J. Polym. Sci.* **1957**, *24*, 301−306.
(13) Fischer, E. W. Stufed- und spiralfömiges Kristallwachstum bei Hochpolymeren. *Z. Naturforsch., A: Phys. Sci.* **1957**, *12*, 753−754.
(14) Alcock, B.; Cabrera, N. O.; Barkoula, N. M.; Peijs, T. The Effect of Processing Conditions on the Mechanical Properties and Thermal Stability of Highly Oriented PP Tapes. *Eur. Polym. J.* **2009**, *45*, 2878−2894.
(15) Wenig, W.; Hammel, R. Optical Properties and Structure of Drawn Polyethyleneterephthalate-Polyethylene Films. *Colloid Polym. Sci.* **1982**, *260*, 31−36.
(16) Koike, Y. High-Bandwidth Graded-Index Polymer Optical Fiber. *Polymer* **1991**, *32*, 1737−1745.
(17) Flory, P. J. On the Morphology of the Crystalline State in Polymers. *J. Am. Chem. Soc.* **1962**, *84*, 2857−2867.
(18) Kim, K. M.; Keum, D. K.; Chujo, Y. Organic-Inorganic Polymer Hybrids Using Polyoxazoline Initiated by Functionalized Silsesquioxane. *Macromolecules* **2003**, *36*, 867−875.
(19) Oliveira, F.; Leterrier, Y.; Månson, J.; Sereda, O.; Neels, A.; Dommann, A.; Damjanovic, D. Process Influences on the Structure, Piezoelectric, and Gas-Barrier Properties of PVDF-TrFE Copolymer. *J. Polym. Sci., Part B: Polym. Phys.* **2014**, *52*, 496−506.
(20) Xu, Z.; Zhang, J.; Shan, M.; Li, Y.; Li, B.; Niu, J.; Zhou, B.; Qian, X. Organosilane-Functionalized Graphene Oxide for Enhanced Antifouling and Mechanical Properties of Polyvinylidene Fluoride Ultrafiltration Membranes. *J. Membr. Sci.* **2014**, *458*, 1−13.
(21) Fujimori, A.; Ninomiya, N.; Masuko, T. Influence of Dispersed Organophilic Montmorillonite at Nanometer-Scale on Crystallization of Poly(L-lactide). *Polym. Eng. Sci.* **2008**, *48*, 1103−1111.
(22) Korobov, M. V.; Avramenko, N. V.; Bogachev, A. G.; Rozhkova, N. N.; Osawa, E. Nanophase of Water in Nano-Diamond Gel. *J. Phys. Chem. C* **2007**, *111*, 7330−7334.
(23) May, P. W. Materials science. The New Diamond Age? *Science* **2008**, *319*, 1490−1491.
(24) Joannopoulos, J. D.; Meade, R. D.; Winn, J. N. *Photonic Crystals*; Princeton University Press: Princeton, NJ, 1995.

DOI: 10.1021/acsami.5b04083
ACS Appl. Mater. Interfaces 2015, 7, 17792−17801

(25) Zanin, H.; May, P. W.; Fermin, D. J.; Plana, D.; Vieira, S. M. C.; Milne, W. I.; Corat, E. J. Porous Boron-Doped Diamond/Carbon Nanotube Electrodes. *ACS Appl. Mater. Interfaces* **2014**, *6*, 990−995.
(26) Ondic, L.; Dohnalova, K.; Ledinsky, M.; Kromka, A.; Babchenko, O.; Rezek, B. Effective Extraction of Photoluminescence from a Diamond Layer with a Photonic Crystal. *ACS Nano* **2011**, *5*, 346−350.
(27) Yu, J.; Qian, R.; Jiang, P. Largely Enhanced Thermal Conductivity for PVDF Composites with a Hybrid Functionalized Graphene Sheet-Nanodiamond Filler. *Fibers Polym.* **2015**, *453*, 169−176.
(28) Lam, R.; Chen, M.; Pierstorff, E.; Huang, H.; Osawa, E.; Ho, D. Nanodiamond-Embedded Microfilm Devices for Localized Chemotherapeutic Elution. *ACS Nano* **2008**, *2*, 2095−2102.
(29) Masuda, H.; Watanabe, M.; Yasui, K.; Tryk, D.; Rao, T.; Fujishima, A. Fabrication of a Nanostructured Diamond Honeycomb Film. *Adv. Mater.* **2000**, *12*, 444−447.
(30) Tong, W.; Fox, K.; Ganesan, K.; Turnley, A. M.; Shimoni, O.; Tran, P. A.; Lohrmann, A.; McFarlane, T.; Ahnood, A.; Garrett, D. J.; Meffin, H.; O'Brien-Simpson, N. M.; Reynolds, E. C.; Prawer, S. Fabrication of Planarised Conductively Patterned Diamond for Bio-Applications. *Mater. Sci. Eng., C* **2014**, *43*, 135−144.
(31) Sharma, M.; Singh, M. P.; Srivastava, C.; Madras, G.; Bose, S. Poly(vinylidene fluoride)-Based Flexible and Lightweight Materials for Attenuating Microwave Radiations. *ACS Appl. Mater. Interfaces* **2014**, *6*, 21151−25160.
(32) Garcia-Segura, S.; Centellas, F.; Brillas, E. Unprecedented Electrochemiluminescence of Luminol on a Boron-Doped Diamond Thin-Film Anode. Enhancement by Electrogenerated Superoxide Radical Anion. *J. Phys. Chem. C* **2012**, *116*, 15500−15504.
(33) Yu, S.-J.; Kang, M.-W.; Chang, H.-C.; Chen, K.-M.; Yu, Y.-C. Bright Fluorescent Nanodiamonds: no Photobleaching and Low Cytotoxicity. *J. Am. Chem. Soc.* **2005**, *127*, 17604−17605.
(34) Tsibouklis, J.; Nevell, T. G. Ultra-Low Surface Energy Polymers: the Molecular Design Requirements. *Adv. Mater.* **2003**, *15*, 647−650.
(35) Thomassin, J. M.; Pagnoulle, C.; Bizzari, D.; Caldarella, G.; Germain, A.; Jérôme, R. Improvement of the Barrier Properties of Nafion by Fluoro-Modified Montmorillonite. *Solid State Ionics* **2006**, *177*, 1137−1144.
(36) Overney, R. M.; Meyer, E.; Frommer, J.; Güntherodt, H. J.; Fujihira, M.; Takano, H.; Gotoh, Y. Force Microscopy Study of Friction and Elastic Compliance of Phase-Separated Organic Thin Films. *Langmuir* **1994**, *10*, 1281−1286.
(37) Bunn, C. W.; Howells, E. R. Structures of Molecules and Crystals of Fluoro-Carbons. *Nature* **1954**, *174*, 549−551.
(38) Runt, J.; Jin, L.; Talibuddin, S.; Davis, C. R. Crystalline Homopolymer-Copolymer Blends: Poly(tetrafluoroethylene)-Poly-(tetrafluoroethylene-co-perfluoroalkylvinyl ether). *Macromolecules* **1995**, *28*, 2781−2786.
(39) Ranieri, J. P.; Bellamkonda, R.; Bekos, E. J.; Vargo, T. G.; Gardella, J. A.; Aebischer, P. Neuronal Cell Attachment to Fluorinated Ethylene Propylene Films with Covalently Immobilizes Laminin Oligopeptides. *J. Biomed. Mater. Res.* **1995**, *29*, 779−785.
(40) Varcoe, J. R.; Slade, R. C. T. An Electron-Beam-Grafted ETFE Alkaline Anion-Exchange Membrane in Metal-Cation-Free Solid-State Alkaline Fuel Cells. *Electrochem. Commun.* **2006**, *8*, 839−843.
(41) Xu, T. Ion Exchange Membranes: State of Their Development and perspective. *J. Membr. Sci.* **2005**, *263*, 1−29.
(42) Fujimori, A.; Kasahara, Y.; Honda, N.; Akasaka, S. The Role of Modifying Molecular Chains in the Formation of Organized Molecular Films of Organo-modified Nanodiamond.: Construction of a Highly-Ordered Low Defect Particle Layer, and Evaluation of Desorption Behavior of Organic Chains. *Langmuir* **2015**, *31*, 2895−2904.
(43) Zanin, H. G.; May, P. W.; Fermin, D. J.; Plana, D.; Vieira, S. M. C.; Milne, W. I.; Corat, E. J. Porous Boron-Doped/Carbon Nanotube Electrodes. *ACS Appl. Mater. Interfaces* **2014**, *6*, 990−995.
(44) Chen, J.; Asano, M.; Yamaki, T.; Yoshida, M. Preparation and Characterization of Chemically Stable Polymer Electrolyte Membranes by Radiation-Induced Graft Copolymerization of Four Monomers into ETFE Films. *J. Membr. Sci.* **2006**, *269*, 194−204.
(45) Fujimori, A.; Arai, S.; Soutome, Y.; Hashimoto, M. Improvement of Thermal Stability of Enzyme via Immobilization on Lanmuir-Blodgett Films of Organo-Modified Aluminosilicate with Higher Coverage. *Colloids Surf., A* **2014**, *448*, 45−52.
(46) Katan, E.; Narkis, M.; Siegmann, A. The Effect of Some Fluoropolymers' Structures on Their Response to UV Irradiation. *J. Appl. Polym. Sci.* **1998**, *70*, 1471−1481.
(47) Brack, H. P.; Bührer, H. G.; Bonorand, L.; Scherer, G. G. Grafting of Pre-Irradiated Poly(ethylene-alt-tetrafluoroethylene) Films with Styrene: Influence of Base Polymer Film Properties and Processing Parameters. *J. Mater. Chem.* **2000**, *10*, 1795−1803.
(48) Parada, M. A.; de Almeida, A.; Muntele, I.; Muntele, C.; Delalez, N.; Ila, D. ETFE Polymer Bombarded with 1 MeV Proton. *Nucl. Instrum. Methods Phys. Res., Sect. B* **2005**, *241*, 517−520.
(49) Chen, J.; Asano, M.; Yamaki, T.; Yoshida, M. Chemical and Radiation Crosslinked Polymer Electrolyte Membranes Prepared from Radiation-Grafted ETFE Films for DMFC Applications. *J. Power Sources* **2006**, *158*, 69−77.
(50) Umemura, A.; Uchida, M.; Hirata, T.; Sato, J. I. Physical Model Analysis of Flame Spreading along an Electrical Wire in Microgravity. *Proc. Combust. Inst.* **2002**, *29*, 2535−2543.
(51) Mathews, A. S.; A, S.; Kim, L.; Ha, C. S. Synthesis, Characterization, and Properties of Fully Aliphatic Polyimides and Their Derivatives for Microelectronics and Optoelectronics Applications. *Macromol. Res.* **2007**, *15*, 114−128.
(52) Osawa, E. Monodisperse Single Nanodiamond Particulates. *Pure Appl. Chem.* **2008**, *80*, 1365−1379.
(53) Forrest, S. R. The Path to Ubiquitous and Low-Cost Organic Electronic Appliances on Plastic. *Nature* **2004**, *428*, 911−918.
(54) Fujimori, A.; Honda, N.; Iwashita, H.; Kaneko, Y.; Arai, S.; Sumita, M.; Akasaka, S. Formation and Structure of Fine Multi-Particle Layered Organo-Modified Zirconium Dioxides Fabricated by Langmuir-Blodgett Technique. *Colloids Surf., A* **2014**, *446*, 109−117.
(55) Fujimori, A.; Kaneko, Y.; Kikkawa, T.; Chiba, S.; Shibasaki, Y. Fabrication and Structure of "Polymer Nanosphere Multilayered Organization. *J. Colloid Interface Sci.* **2014**, *418*, 338−349.
(56) Chen, X.; Tian, X.; Zhou, Z.; Jiang, M.; Lu, J.; Wang, Y.; Wang, L. Effective Improvement in Microwave Absorption by Uniform Dispersion of Nanodiamond in Polyaniline through In-situ Polymerization. *Appl. Phys. Lett.* **2015**, *106*, 233103.
(57) Zhang, W.; Zhang, Z.; Yang, J.; Huang, T.; Zhang, N.; Zheng, X.; Wang, Y.; Zhou, Z. Largely Enhanced Thermal Conductivity of Poly(vinylidene fluoride)/Carbon Nanotube Composites Achieved by Adding Graphene Oxide. *Carbon* **2015**, *90*, 242−254.
(58) Hayasaka, Y.; Tamura, T.; Fujimori, A. Fine Structure of Fluorinated Copolymer/Nano-Filler Composites. *Trans. Mater. Res. Soc. Jpn.* **2008**, *33*, 137−140.
(59) Teyssedre, G.; Bernes, A.; Lacabanne, C. Cooperative Movements Associated with the Curie Transition in P(VDF-TrFE) Copolymers. *J. Polym. Sci., Part B: Polym. Phys.* **1995**, *33*, 879−890.
(60) Kochervinskii, V. V.; Kozlova, N. V.; Khnykov, A. Y.; Shcherbina, M. A.; Sulyanov, S. N.; Dembo, K. A. Features of Structure Formation and Electrophysical Properties of Poly(vinylidene fluoride) Crystalline Ferroelectric Polymers. *J. Appl. Polym. Sci.* **2009**, *116*, 695−707.
(61) Datta, J.; Nandi, A. K. Cocrystallization of Poly (vinylidene fluoride) and Vinylidene Fluoride-Tetrafluoro-Ethylene Copolymer Blends: 3. Structural Study. *Polymer* **1997**, *38*, 2719−2724.
(62) Guiner, A. *International Tables for X-ray Crystallography*; Kynoch Press: Birmingham, U.K., 1968.
(63) Strobl, G. R.; Schneider, M. Direct Evaluation of the Electron Density Correlation Function of Partially Crystalline Polymers. *J. Polym. Sci., Polym. Phys. Ed.* **1980**, *18*, 1343−1359.
(64) Stroble, G. R. *The Physics of Polymers*; Springer: Berlin, Germany, 1997; Vol. *408*.
(65) Nam, P. H.; Ninomiya, N.; Fujimori, A.; Masuko, T. Less-Ordered Lamellar Structure of Intercalated Poly(L-lactide)/Organo-

DOI: 10.1021/acsami.5b04083
ACS Appl. Mater. Interfaces 2015, 7, 17792−17801

Modified Montmorillonite Hybrids. *Polym. Eng. Sci.* **2006**, *46*, 703−711.
(66) Ozawa, T. A New Method of Analyzing Thermogravimetric Data. *Bull. Chem. Soc. Jpn.* **1965**, *38*, 1881−1886.
(67) Nagasawa, S.; Fujimori, A.; Masuko, T.; Iguchi, M. Crystallisation of Polypropylene Containing Nucleators. *Polymer* **2005**, *46*, 5241−5240.
(68) Nyuui, T.; Isawa, O.; Fujimori, A. Nucleator Effect to the Crystallization Behavior of Perfluorinated Copolymers. *Netsu Sokutei* **2011**, *38*, 77−82.

DOI: 10.1021/acsami.5b04083
ACS Appl. Mater. Interfaces 2015, 7, 17792−17801